Analytical Model Development and Impulse Thrusters Pairing Guidelines for Trajectory Corrections of Spin-Stabilized Projectiles

Daniel Corriveau[1]
Defence R&D Canada - Valcartier, Quebec City, QC, G3J 1X5, Canada

Pierre Wey[2] and Claude Berner[3]
French-German Research Institute of Saint-Louis, Saint-Louis, 68300, France

A novel method for correcting the trajectory of artillery projectile using pairs of impulse thrusters is described in this paper. Standard thruster-guided spin-stabilized projectile usually incorporates squibs at the center-of-mass in order to avoid generating yaw and thus increasing the drag. However, by locating the impulse thrusters aft of the center-of-mass, it is possible to increase significantly the correction in drift. This is explained by the fact that in such case, the deflection results from the aerodynamic jump due to the projectile oscillation in addition to that of the impulses when the thruster is located aft of the projectile. In order to benefit from the added drift correction obtained by locating the thrusters away from the center-of-mass and avoid the added drag generated by the induced pitching and yawing motion, an optimal combination of thruster can be achieved by considering pairs of impulses which have the double objective of maximizing the deflection and minimizing the drag due to the oscillations. In this paper, the linear theory of ballistic is used to develop an analytical model representing the motion of a projectile subjected to impulse thrusters. Using the linearized equations of angular motion and considering ideal cases, the optimization scheme for using double impulses is defined by three rules. The latter are then assessed in the case of actual projectiles, using 6-DOF computations.

Nomenclature

a	=	angular deflection of the trajectory
A	=	projectile reference area [m^2] (= $\pi d^2/4$)
$C_{L\alpha}$	=	lift force coefficient
$C_{m\alpha}$	=	pitching moment coefficient
C_D	=	drag coefficient
$C_{Mp\alpha}$	=	Magnus moment coefficient
C_{mq}	=	pitching damping moment coefficient
d	=	projectile reference caliber [m]
I_x	=	projectile axial moment of inertia [kg·m^2]
I_y	=	projectile transverse moment of inertia [kg·m^2]
J	=	impulse vector due to the thruster [N·s]
J_{D_2}	=	impulse vector due to the quadratic-yaw drag force [N·s]
J_L	=	impulse vector due to the lift force [N·s]
J_Y	=	impulse vector due to the Magnus force [N·s]
K_{S0}, K_{F0}	=	initial amplitude of the slow and fast epicyclic yaw arm

[1] Defence Scientist, Precision Weapon Section, 2459 Pie-XI Blvd. North, Quebec City.
[2] Research Scientist, Aeromechanics and Acoustics Division, 5 rue du Général Cassagnou, Saint-Louis.
[3] Research Scientist, Aeromechanics and Acoustics Division, 5 rue du Général Cassagnou, Saint-Louis.

l_{CJ} = distance from center of mass to location of applied impulse [cal] (positive towards nose, negative towards boattail)
m = projectile mass [kg]
p = projectile axial spin [s^{-1}]
s = distance traveled along the flight path [cal]
V = projectile velocity [$m \cdot s^{-1}$]
$\overline{\alpha}$ = total incidence angle
α = pitch angle
β = yaw angle
ϕ = orientation of vectors defined in the (α, β) frame
ξ = complex incidence $\xi = \alpha + i\beta = |\xi| e^{i\phi}$
ξ_0' = initial yaw rate [rad/s]
ξ_0 = initial yaw [rad]
ρ = air density [kg/m^3]
λ_S, λ_F = slow and fast arm damping rate [1/m]
ϕ_S', ϕ_F' = slow and fast arm turning rate [rad/s]

I. Introduction

A collaborative project between the French-German Research Institute of Saint-Louis (ISL) and Defence R&D Canada has the objective of better understanding the use of impulsers on artillery projectiles and their impact on the aerodynamics of these ammunitions. The impulse thrusters consist of small detonators that generate a high force for a very short period of time. The impulse thrusters differ significantly from the more conventional jet thrusters in that the impulse is created by the detonation of explosive material as opposed to accelerating a gas through a nozzle. The impulsers are being developed and manufactured at ISL. The thrusters will be mounted inside the projectile at a specific axial location in a ring-like fashion. They will be used to divert the projectile laterally.

Research and development on the use of thrusters or reaction jets to improve the precision of fin stabilized projectiles such as missiles and rockets has been going on for decades now. Over the years, a significant amount of research was performed to understand the interaction of the reaction jets with the projectile's external flow as demonstrated by Champigny and Lacau [1]. Furthermore, several investigators studied the loads caused by lateral pulse jets on projectile body. Brandeis and Gill [2] performed an experimental study on the effect of a lateral jet on the forces and moments on a supersonic missile. Recently, trajectory corrections using impulsers have been investigated at ISL for a project on a guided supersonic finned projectile [3].

For spin stabilized projectiles, the use of impulsers or jet thrusters is not as common so the technology is still very much into the development phase. Horwath and Barnych [4] presented a concept of a Low Cost Course Correction (LCCC) technique applied to a 40 mm projectile that makes use of impulsers. Magnotti et al. [5] tested similar LCCC fuzes on an experimental mortar projectile. Flight path corrections of up to 6.0 mils were obtained using an impulse of 2.6 Ns.

Research on the impact of thrusters or impulsers on the flight dynamics of spinning projectiles is very scarce in the open literature. Using the projectile linear theory, Cooper [6] has shown analytically that the effect of an impulse on a spinning projectile was to produce an additive contribution to the usual aerodynamic jump of the free-flight projectile with no applied impulse. Burchett et al. [7] developed closed-form expressions for the swerving motion of a dual-spin projectile in atmospheric flight under the action of lateral pulse jets.

Research and development is currently ongoing in order to increase the magnitude of the impulse generated by thrusters and also to reduce the size of these devices. An example of such work is that of English et al. [8] who developed a high-power, short-duration MEMs-sized gas generator actuator for spinning projectiles.

The objective of this study consists in developing a control scheme for the control of artillery projectiles using pairs of impulse thrusters. In the first part of the paper, the concept of impulse pairing to achieve effective control of a spin-stabilized projectile is introduced. The theoretical background of the pairing method is explained in the case of ideal projectiles. Three basic rules are presented to ensure successful pairing of impulse thrusters to maximize lateral corrections.

The second part of the paper presents the results from 6-DOF computations applied to the actual parameters of a generic 105mm artillery shell. Compared to the analytical results presented in Wey and Corriveau [9], 6-DOF computations take into account the variations in the projectile velocity and aerodynamic coefficients during the flight. These simulations serve to validate the use of the impulse pairing process as a viable projectile control alternative.

II. Analytical Model

Using the linear theory of ballistics, an analytical model was developed in order to predict the projectile's angular motion and velocity resulting from the activation of thrusters. Neglecting the steady-state yaw due to the gravity, introducing the effect of the impulse and shifting the origin of the flight path to the impulse location, the epicyclic pitching and yawing motion of a projectile can be represented by the following differential equation (McCoy [10]):

$$\xi'' + (H - iP)\xi' - (M + iPT)\xi = \xi_0' \delta(s) \tag{1}$$

where $\xi = \alpha + i\beta$ (see Fig. 1) is the complex incidence and the superscript prime denotes differentiation with respect to the flight path s. $\delta(s)$ is the Dirac function. The coefficient H, P, M and T are defined as follows:

$$H = \frac{\rho A d}{2m}\left(C_{L_\alpha} - C_D - \frac{md^2}{I_y} C_{M_q}\right) \tag{2}$$

$$P = \frac{I_x}{I_y}\frac{pd}{V} \tag{3}$$

$$M = \frac{\rho A d^3}{2I_y} C_{M_\alpha} \tag{4}$$

$$T = \frac{\rho A d}{2m}\left(C_{L_\alpha} + \frac{md^2}{I_x} C_{M_{p\alpha}}\right). \tag{5}$$

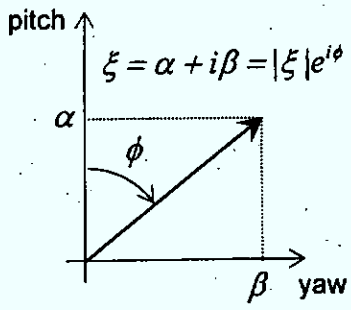

Figure 1. Complex incidence.

The solution to Eq. (1) is given by the sum of the Slow and Fast arms (denoted *S* and *F*, respectively) of the epicyclic motion as follows:

$$\xi = K_{F_0} e^{\left(\lambda_F s + i\left(\phi'_F s + \phi_{F_0}\right)\right)} + K_{S_0} e^{\left(\lambda_S s + i\left(\phi'_S s + \phi_{S_0}\right)\right)} \tag{6}$$

In this equation, ϕ'_F and ϕ'_S are the fast and slow arm turning rates whereas λ_F and λ_S are the fast and slow arm damping exponents. These are defined as follows:

$$\phi'_F = \frac{1}{2}\left(P + \sqrt{P^2 - 4M}\right) \tag{7}$$

$$\phi'_S = \frac{1}{2}\left(P - \sqrt{P^2 - 4M}\right) \tag{8}$$

$$\lambda_F = -\frac{1}{2}\left(H - \frac{P(2T - H)}{\sqrt{P^2 - 4M}}\right) \tag{9}$$

$$\lambda_S = -\frac{1}{2}\left(H + \frac{P(2T - H)}{\sqrt{P^2 - 4M}}\right) \tag{10}$$

The initial amplitudes and phase angles of the fast and slow arms are defined by the initial conditions of the yaw motion as follows:

$$K_{F_0} e^{i\phi_{F_0}} = -\frac{i\xi'_0 + \phi'_S \xi_0}{\phi'_F - \phi'_S} \tag{11}$$

$$K_{S_0} e^{i\phi_{S_0}} = \frac{i\xi_0' + \phi_F' \xi_0}{\phi_F' - \phi_S'} \quad (12)$$

In Eq. (11) and (12), the initial incidence of the projectile following an impulse thruster detonation of magnitude J and orientation ϕ_J can estimated from the ratio of the impulse's momentum and the projectile's momentum:

$$\xi_0 = \frac{1}{mV} J e^{i\phi_J} \quad (13)$$

The initial yaw rate can be obtained from a balance of the angular momentum:

$$\xi_0' = \frac{L_J d^2}{I_y V} J e^{i\phi_J} \quad (14)$$

Using the analytically derived equation for the complex incidence (Eq. (6)), the complex deflection velocity $V_L e^{i\phi_{V_L}}$ due to the lift force L resulting from the yawing motion can be computed as:

$$J_L = mV_L e^{i\phi_{V_L}} = \int_0^\infty L(t)\,dt = \int_0^\infty L(s)\frac{d}{V}ds = \int_0^\infty \left(\frac{1}{2}\rho A V^2 C_{L_\alpha} \xi\right)\frac{d}{V}ds = \frac{1}{2}\rho A V d C_{L_\alpha} \int_0^\infty \xi\, ds \quad (15)$$

The difference between ϕ_J and ϕ_{V_L} is the included angle between the axes defined by J and J_L. It can reach a few degrees for a standard artillery shell. Thus, the vectors J and J_L are roughly aligned along the same axis, either in the same direction or in opposite directions.

Similarly, the loss of velocity V_{D_2} due to the additional drag D_2 resulting from the yaw motion can be defined as:

$$J_{D_2} = mV_{D_2} = \int_0^\infty D_2(t)\,dt = \int_0^\infty D_2(s)\frac{d}{V}ds = \int_0^\infty \left(\frac{1}{2}\rho A V^2 C_{D_2} |\xi|^2\right)\frac{d}{V}ds = \frac{1}{2}\rho A V d C_{D_2} \int_0^\infty |\xi|^2\, ds \quad (16)$$

assuming that $C_D = C_{D_0} + C_{D_2}|\xi|^2$.

The definite integral ξ and $|\xi|^2 = \xi\bar{\xi}$ in Eq. (15) and (16) are given by:

$$\int_0^\infty \xi\, ds = -\frac{K_{F_0} e^{i\phi_{F_0}}}{\lambda_F + i\phi_F'} - \frac{K_{S_0} e^{i\phi_{S_0}}}{\lambda_S + i\phi_S'} \quad (17)$$

$$\int_0^\infty |\xi|^2 ds = -\frac{K_{F_0}^2}{2\lambda_F} - \frac{K_{S_0}^2}{2\lambda_S} - \frac{2K_{F_0}K_{S_0}\left[(\lambda_F+\lambda_S)\cos(\phi_{F_0}-\phi_{S_0})+(\phi'_F-\phi'_S)\sin(\phi_{F_0}-\phi_{S_0})\right]}{(\lambda_F+\lambda_S)^2+(\phi'_F-\phi'_S)^2} \tag{18}$$

assuming that $\lambda_F < 0$ and $\lambda_S < 0$.

Substituting Eq. (17) in Eq. (15), the lift impulse or aerodynamic jump can be rewritten as:

$$J_L = -\frac{1}{2}\rho AV d C_{L_\alpha}\left[\frac{K_{F_0}e^{i\phi_{F_0}}}{\lambda_F + i\phi'_F} + \frac{K_{S_0}e^{i\phi_{S_0}}}{\lambda_S + i\phi'_S}\right] \tag{19}$$

or

$$J_L = -\frac{1}{2}\rho AV d C_{L_\alpha}\left[\left(\frac{\lambda_F - i\phi'_F}{\lambda_F^{\,2}+\phi_F'^{\,2}}\right)K_{F_0}e^{i\phi_{F_0}} + \left(\frac{\lambda_S - i\phi'_S}{\lambda_S^{\,2}+\phi_S'^{\,2}}\right)K_{S_0}e^{i\phi_{S_0}}\right] \tag{20}$$

As mentioned by McCoy [11], the damping exponents are in general between one and two orders of magnitude smaller than the epicyclic turning rates. Thus, a very decent approximation to Eq. (20) can be written as follows:

$$J_L = i\frac{1}{2}\rho AV d C_{L_\alpha}\left[\frac{K_{F_0}}{\phi'_F}e^{i\phi_{F_0}} + \frac{K_{S_0}}{\phi'_S}e^{i\phi_{S_0}}\right]. \tag{21}$$

Substituting Eq. (11) and (12) into Eq. (21) one obtains:

$$J_L = i\frac{1}{2}\rho AV d C_{L_\alpha}\left[\frac{-i\xi'_0 - \phi'_S\xi_0}{\phi'_F(\phi'_F-\phi'_S)} + \frac{i\xi'_0 + \phi'_F\xi_0}{\phi'_S(\phi'_F-\phi'_S)}\right] \tag{22}$$

Now, $M = \phi'_F\,\phi'_S - \lambda_F\,\lambda_S = \frac{\rho A d^3}{2I_y}C_{m\alpha} \approx \phi'_F\,\phi'_S$ and $P = \phi'_F + \phi'_S$. Substituting these in Eq. (22), the following is obtained:

$$J_L = i\frac{1}{2}\rho AV d C_{L_\alpha}\left[\frac{-i\xi'_0 + P\xi_0}{M}\right] \tag{23}$$

$$J_L = V \frac{I_y}{d^2} \frac{C_{L_\alpha}}{C_{m_\alpha}} \left[iP\xi_0 - \xi_0' \right] \tag{24}$$

III. Impulse Optimization Technique

A. Single Impulse

In order to optimize the use of impulse on spin-stabilized projectile, a projectile of mass m traveling at velocity V is considered. A Dirac impulse J is engaged at some travel distance s. The impulse vector is normal to the projectile axis and is applied aft of the center-of-gravity. This event forces the oscillation of the projectile which yields three impulses due to the aerodynamic forces as shown in Figure 2: two transverse impulses J_L and J_Y due to the action of the lift and Magnus forces and one axial impulse J_{D2} due to the squared-yaw component of the drag force. Assuming a constant velocity V, the total angular deflection of the trajectory is then simply given by:

$$a = \frac{J + J_L + J_Y}{mV} \tag{25}$$

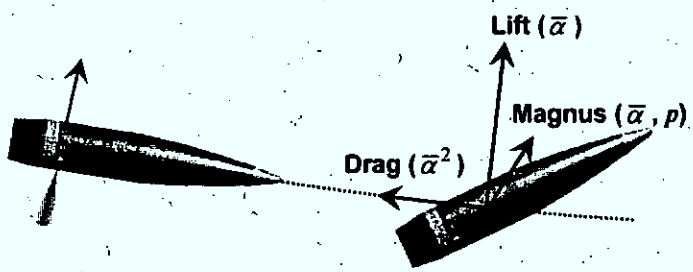

Figure 2. Forces due to the total incidence, $\bar{\alpha}$.

In order to maximize the angular deflection, the sum of the impulse $J+J_L$ must be maximized in Eq. (25). This can be achieved if the thruster impulse J and the resulting lift impulse J_L are aligned in the same direction. For a spin-stabilized shell, this condition is met if the impulse thrusters are fired behind the center of mass as shown in Figure 3. This can be demonstrated physically by looking at Figure 4. In this figure, a thruster is triggered on the port side of the projectile resulting in a rightward pointing impulse J. This impulse initiates the angular motion of the projectile. The resulting initial yaw rate ξ_0' and the initial angular motion of the projectile are to the left.

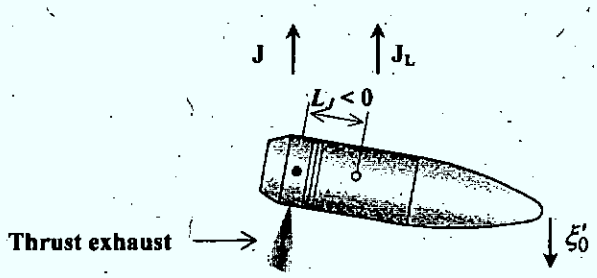

Figure 3. Spin-stabilized configuration.

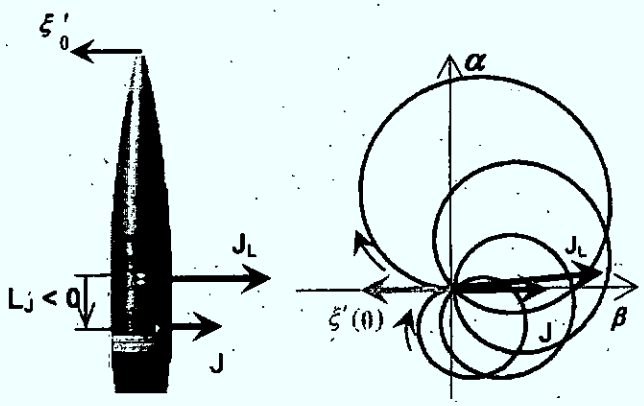

Figure 4. Effect of an impulse on the projectile's angular motion.

However, the gyroscopic response rapidly pitches up the nose of the projectile and eventually the resulting yaw motion is primarily oriented to the right of the projectile. Therefore, the net lift impulse J_L is oriented in the same direction as the thruster impulse to the right as shown in Figure 4. Assuming that ξ_0' is the major cause of the forced epicyclic motion, the relation between the lift impulse J_L and the thruster impulse J can be derived by substituting Eq. (14) into Eq. (24). This yield the following relationship between J and J_L:

$$J_L = -J L_J \frac{C_{L\alpha}}{C_{m\alpha}} e^{i\Delta\phi_J} \tag{26}$$

where $\Delta\phi_J$ is the included angle between the axes defined by J and J_L. Assuming that ξ_0' is the major cause of the forced epicyclic motion, $\Delta\phi_J$ is few degrees for a standard artillery shell. Thus, the vectors J and J_L are roughly aligned along the same axis.

In order to maximize $J+J_L$, Rule#1 must be observed:

Rule#1:

The impulse must be applied behind the center of mass for spin-stabilized projectiles ($L_J < 0$ and $C_{m\alpha} > 0$).

Rule#1 was previously illustrated in Figures 3 and 4.

B. Paired Impulse

Pairing the impulses has the double objective of maximizing the trajectory deflection and minimizing the additional drag due to the forced oscillation. Consider two Dirac impulses J_1 and J_2 that are engaged at travel distances s_1 and s_2. Both impulse vectors are normal to the projectile axis and are applied at L_{J1} and L_{J2} calibers from the center of mass. Within the frame of the linearized equation of the angular motion, the resulting complex angle is simply defined as $\xi = \xi_1 + \xi_2$ where ξ_1 and ξ_2 are phase shifted epicyclic motions having the same frequencies but different initial conditions as shown in Figure 5.

Under the assumption of linearity, the total deflection angle is:

$$a = \frac{J_1 + J_{1L} + J_{1Y} + J_2 + J_{2L} + J_{2Y}}{mV} \tag{27}$$

The angle a is independent of s_1 and s_2: it only depends on the orientation of each vector. This leads to Rule#2:

Rule#2:

The transverse impulse is a maximum if J_1 and J_2 are aligned, assuming that L_{J1} and L_{J2} both satisfy Rule#1.

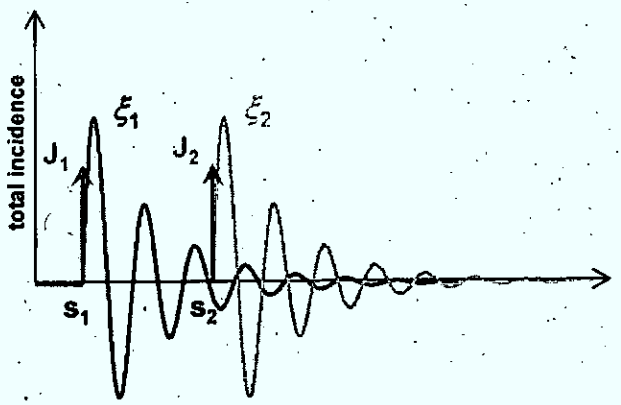

Figure 5. Phase shifted epicyclic motion.

The second impulse should ideally stop the angular motion triggered by the first one. Thus, ξ_1 and ξ_2 should have the same amplitudes and be in opposite phase. For simplicity, we will examine here ideal motions for which ξ_0 can be neglected and having equal damping factors (i.e. $\lambda_F = \lambda_S$). In this case, the epicyclic motions periodically pass through zero because the fast and slow arms always have the same length. The motions are strictly opposed if the following conditions are met:

$$\xi_1(s_2 - s_1) = \xi_2(0) = 0 \tag{28}$$

$$\xi_1'(s_2 - s_1) = -\xi_2'(0) \tag{29}$$

where the origin of each motion has been shifted to the respective impulse locations. Eq. (28) yields the first constraint:

$$s_2 - s_1 = \frac{2k\pi}{\phi_F' - \phi_S'} \tag{30}$$

where k is an integer > 0. Eq. (29) defines J_2 and adds two constraints on s_2:

$$J_2 L_{J2} = J_1 L_{J1} e^{\lambda_F (s_2 - s_1)} \tag{31}$$

$$s_2 - s_1 = \frac{(2k_S + 1)\pi}{\phi'_S} = \frac{(2k_F + 1)\pi}{\phi'_F} \tag{32}$$

where k_S and k_F are integers. Eq. (31) takes into account the damping factor of the motion, which might actually be ignored when dealing with the actual impulse thrusters. Note that Eq. (31) is consistent with Rule#2 since it implies that J_1 and J_2 are aligned.

For spin-stabilized projectiles, we have $\phi'_F > \phi'_S > 0$. In this case, making $k_S = 0$ to minimize s_2, Eq. (32) requires that $\phi'_F = (2k_F + 1)\phi'_S$. Assuming that this ideal condition is satisfied, Eq. (30) is obviously satisfied if $k = k_F$.

These results are summarized by the rule#3:

Rule#3:

$$\boxed{k = \text{nearest integer to} \frac{\text{sign}(\phi'_S)}{2}\left(\frac{\phi'_F}{\phi'_S} - 1\right)} \tag{33}$$

Eq. (33) states that the main condition is to trigger the second impulse at minimum angle of attack. The subordinate condition is to shift the second impulse so that it balances the epicyclic motion as much as possible.

An example of the ideal angular motions created by a pair of sidewise impulses is illustrated in the following figure. Figure 6 shows the generic results for a spinning artillery shell (k=4).

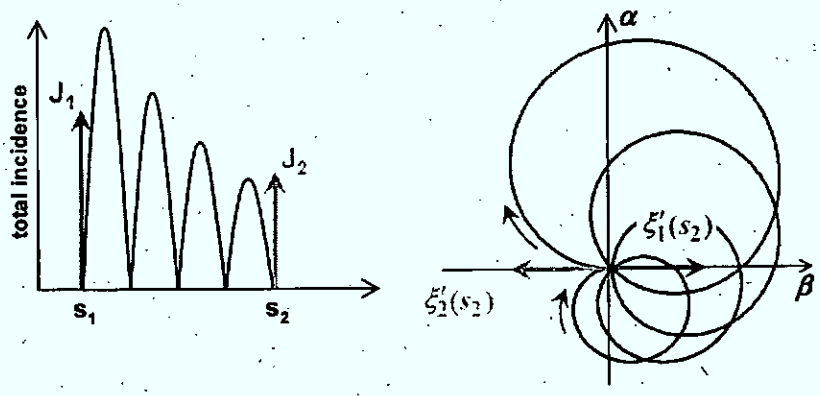

Figure 6. Pairing of two impulses to stop the projectile's angular motion.

IV. Numerical Procedure and Projectile Configuration

A. PRODAS and CONTRAJ Module

The 6-DOF simulations performed as part of this work were done using PRODAS (PROjectile Design/Analysis System). PRODAS provides an effective semi-empirical tool that allows for the rapid and complete design of projectiles. The projectile used for the simulation was modeled using PRODAS model editor. The aerodynamic coefficients used for the trajectory simulations are those predicted by the Spinner2004 module of PRODAS. The aerodynamic predictions of PRODAS are based in part on prior experimental testing through the use of a projectile database. In order to improve the reliability of the aerodynamic model, form factors were used to match the drag coefficients to that obtained from radar traces. Additional adjustments to the aerodynamic coefficients were made in order to match the official firing table for the reference projectile used.

The trajectory simulations were performed using the CONTRAJ module of PRODAS. This is a six Degree-Of-Freedom (6DOF) control flight simulation program developed to simulate flight performance, evaluate trade-offs, and provide estimates of operational capability and limitation for projectile equipped with thrust or impulse control. The impulse thrusters' parameters include the start time, the duration, the thrust, the axial location, the tilt and roll angles.

B. Projectile Configuration

The baseline projectile configuration used for this project is shown in Figure 6. It consists of a 105 mm M1 artillery projectile. The nominal projectile weight is 15.0 kg and its length 494 mm. The muzzle velocity of the projectile was taken to be 506 m/s, which is essentially that obtained when launched from the LG1 MK2 Howitzer. The spin rate of the projectile was set at 1682 rad/s.

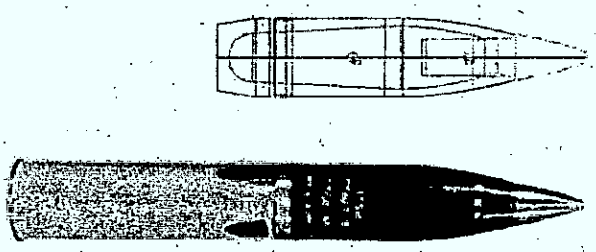

Figure 7. 105 mm M1 artillery projectile together with the PRODAS model used for the simulation.

V. Results and Discussion

The analytical model previously developed in Section II forms the basis of the control by successive impulses. This model needs to predict the motion of the projectile very accurately in order for the control algorithm to detonate the thruster at the right time and roll orientation. In Fig. 8, a comparison between the incidence variations with range of the projectile obtained using 6-DOF simulation and using the analytical model is shown. For this test case, a 10 Ns impulse thruster J_1 was first detonated and a second impulse J_2 was triggered 136m downstream as determined using the three rules presented previously. Comparisons of the incidence variation with range for both the analytical method and the 6-DOF simulation show that there is a slight discrepancy of about 0.1°. However, it can be shown that this difference corresponds essentially to the yaw of repose which is not taken into account in the analytical solution. Other than that, the analytical model predicts the angular motion of the projectile very well.

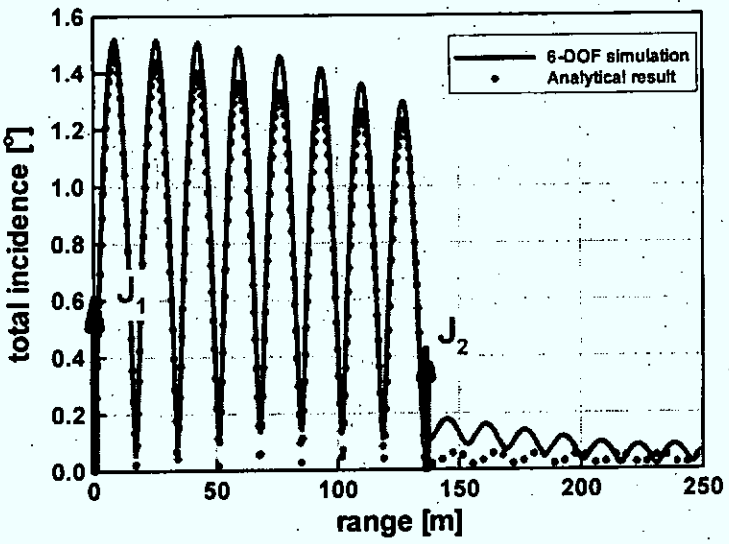

Figure 8. Incidence variation with range following the detonation of 10Ns impulse thruster J_1 and a 7.83Ns impulse thruster J_2.

In Fig. 9, a comparison between the lateral velocity predicted by the analytical model and that predicted by a 6-DOF simulation is shown. The error in the predicted lateral velocity reaches a maximum of the order of 8% following the second impulse. This translates in a lateral velocity error of around 0.1m/s which should be sufficient to ensure adequate accuracy at the target.

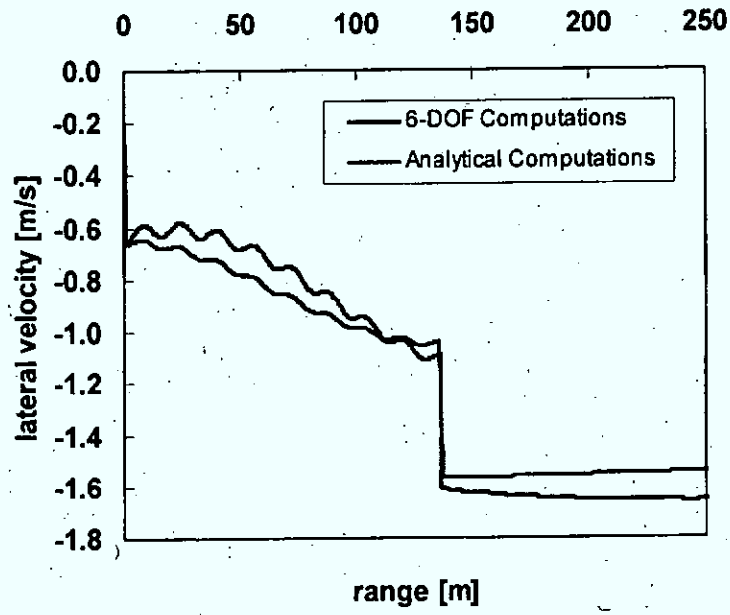

Figure 9. Lateral velocity variation with range following the detonation of 10Ns impulse thruster J_1 and a 7.83Ns impulse thruster J_2.

As mentioned previously, one of the main goals of this study was to establish a procedure for using paired impulse thrusters mounted on an artillery projectile. In order to demonstrate the importance of Rule#1, which requires the impulse thrusters to be located aft of the center of gravity, simulations were performed using a single thruster located along the projectile body. The capacity of this single impulser to alter the trajectory of the projectile in drift was achieved by varying the axial location of the impulser along the projectile body on both the port and starboard sides. An impulse of 10 Ns was used for these simulations. The impulse thruster was triggered just past the apogee on the downward part of a 10000 m ballistic trajectory. The results of that study are presented in Fig. 10. Initially, simulations were performed with an impulse thruster located on the port side of the projectile (left side when looking from behind), thus contributing to an increase in the projectile's drift. The results are presented in Fig. 10, and correspond to the filled symbols. From this figure, it can clearly be seen that the efficiency of the impulser at correcting the trajectory increases significantly when positioned further aft on the projectile body. The importance of Rule#1 is therefore confirmed.

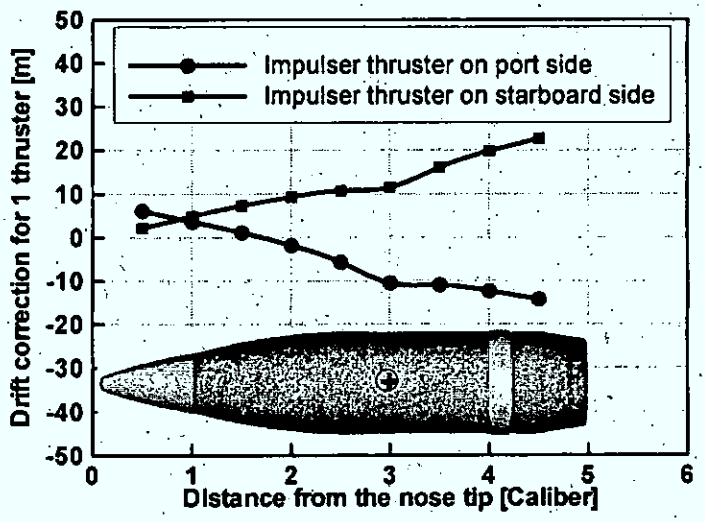

Figure 10. Drift correction as a function of nose tip distance for a 10 Ns impulse thruster triggered at the apogee of a 10000 m trajectory.

The second rule that must followed in order to properly pair two impulse thrusters states that their orientation must be more or less the same in order to maximize the desired correction. In Figure 11, the lateral velocity variation with range is shown for a 10 Ns impulse triggered on the port side of the 105 mm artillery projectile. This impulse generates a lateral velocity V_{J1} and induces a lift velocity V_L due to the angular motion. A second impulse is then triggered at the same roll orientation as the first impulse. The magnitude of this second impulse is slightly less than that of the first impulse in order to take into account the damping of the epicyclic motion as explained previously. As seen from Figure 11, the second impulse, being oriented in same direction as the first impulse, increases the total lateral velocity by an amount almost equal to that of the first one. The final total lateral velocity from this sequence of two-paired lateral impulses is about 1.6 m/s.

In Fig. 12, the same example is repeated but this time the second impulse is detonated in a direction opposite to the first one. As seen in Fig. 12, the second impulse reduces the lateral velocity in such a way that the resulting velocity is significantly less than for the case where the two impulses were oriented in the same direction.

This example clearly shows the importance of detonating the impulses at the same roll orientation in order to maximize the drift velocity correction and hence the drift correction.

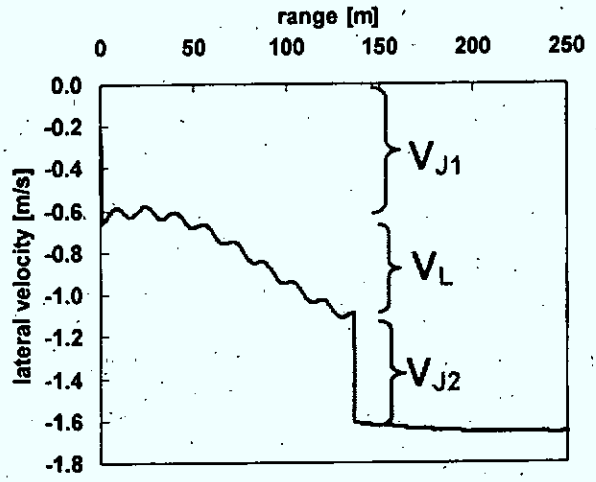

Figure 11. Lateral velocity variation with range for two 10 Ns impulse thrusters fired in the same orientation.

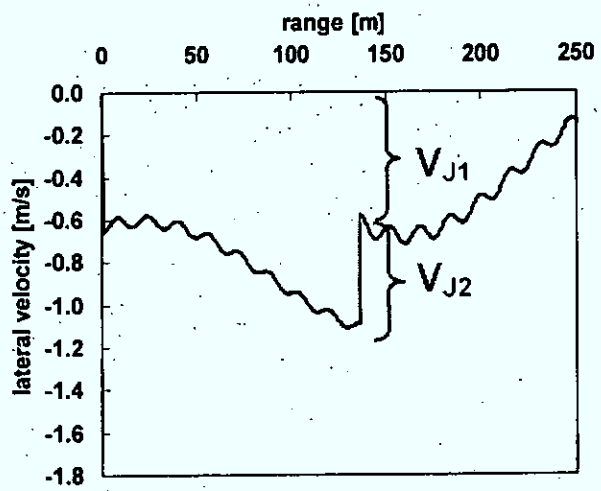

Figure 12. Lateral velocity variation with range for two 10 Ns impulse thrusters fired in opposite orientation.

The third and last rule that must be followed in order to properly pair two impulsers is concerned with the timing between the two impulses. If the two impulse thrusters are properly timed the desired drift correction will be maximized and the angular motion will be stopped.

In Figure 13, the variation of the total incidence with range is shown for a shell fired at an elevation of 10 degrees and a muzzle velocity of 506.3m/sec (Ma 1.49). A 10Ns impulse (J_1) was triggered 0.51cal behind the shell center-of-gravity on the port side at the gun muzzle exit. In order to balance the epicyclic motion and thus reduce drastically the oscillations, a second impulse was fired after 8 cycles of the fast epicycle arm as obtained from Eq. (33) and at the same location and angular position on the shell body. This corresponds to a range of 135.6m downstream of the first impulse as computed from Eq. (30). The magnitude of this impulse was 7.83Ns as computed

from Eq. (31). As seen from Fig. 13 and 14, the angular motion completely stopped following the firing of the second impulse thruster.

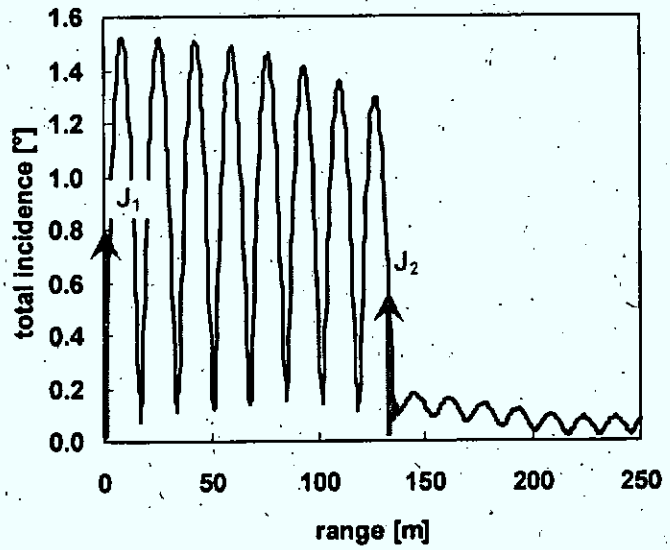

Figure 13. Total incidence variation with range for a 105 mm artillery following the detonation of a pair of impulse thrusters fired according to the three rules.

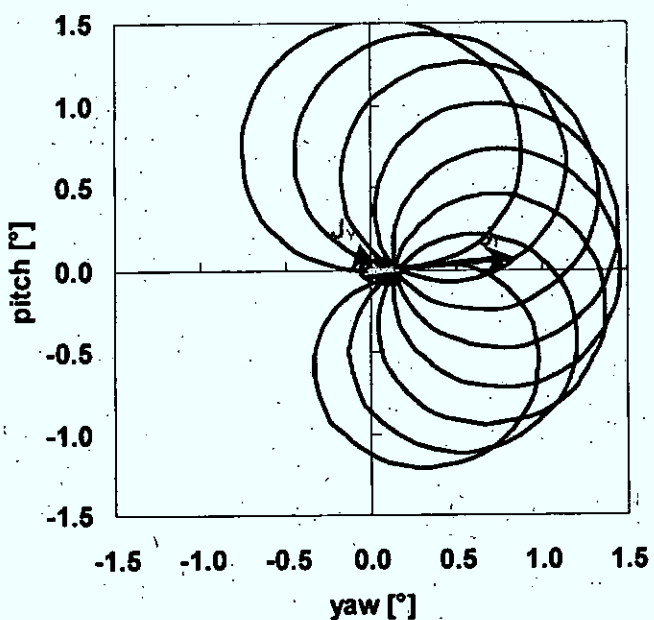

Figure 14. Pitch versus yaw variation with range for a 105 mm artillery following the detonation of a pair of impulse thrusters fired according to the three rules.

Simulations were performed to show the magnitude of the drift correction that can be expected when using paired impulses of 10 Ns and 20 Ns compared to the naturally occurring projectile's drift. The results are shown in Figure 15 and are for the same conditions as those described previously for Figures 13 and 14. The green curve, labelled 0 Ns, is the standard projectile trajectory in drift. The red curve was obtained by triggering a 10 Ns thruster at the gun muzzle followed by a 7.83 Ns thruster 136 m downstream. Finally, the blue trajectory is the result of a 20 Ns impulse and a 15.66 Ns impulse fired on the port side of the projectile.

The drift correction obtained using the 10 Ns impulse pair is about 15 m whereas it is of the order of 30 m for the 20 Ns impulse pair. This appears to be more than sufficient to correct for errors in drift as the Drift Error Probable (DEP) is 3 m for this projectile at 5000m.

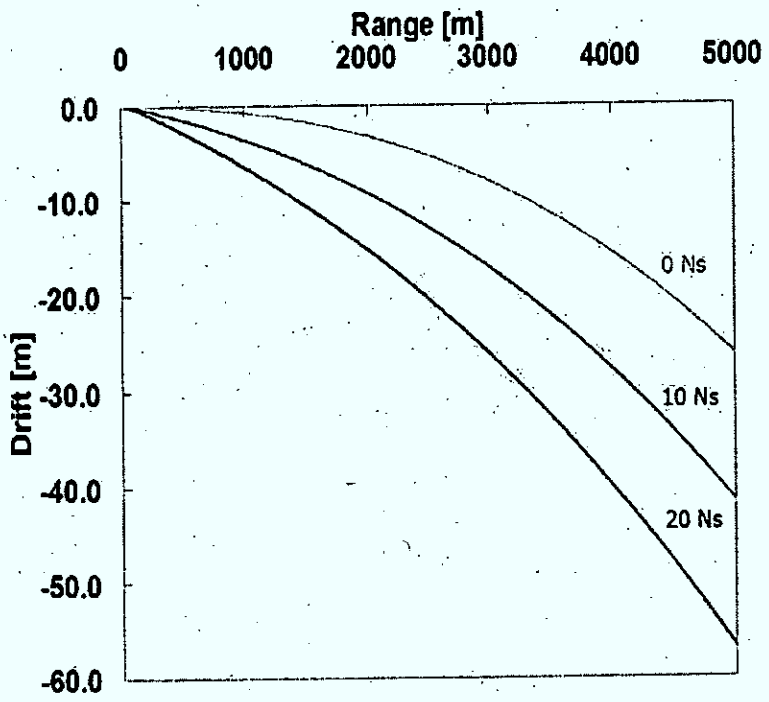

Figure 15. Drift variation with range for a 105 mm artillery fired at 5000 m and subjected to paired impulses of different magnitudes.

VI. Conclusions

A technique to properly pair impulse thrusters on spin-stabilized projectile in order to maximized drift correction while minimizing the range lost due to the angular motion was presented in this paper together with an analytical model used to predict the angular motion of a spin-stabilized projectile following the detonation of an impulse thruster. The analytical model was shown to predict fairly accurately the projectile angular motion and lateral velocity.

The impulse pairing technique consists of essentially following three rules that specify the location of the impulse on the projectile relative to the center-of-gravity, the orientation of the impulses relative to one another and the timing between the two impulses. 6-DOF simulations were performed on a 105 mm M1 artillery projectile using the CONTRAJ module of PRODAS. The aim of these simulations was to demonstrate the importance of following the three rules established in order to properly pair impulse thrusters. Simulations were performed for various location of the thrusters along the projectile's body. Results from these simulations clearly show that the greatest

drift corrections are obtained when the thrusters are located aft of the center-of-gravity as suggested by the first rule. The importance of firing impulses at the same roll orientation was also demonstrated using 6-DOF simulations. The effect of properly timing the second impulse of a pair of thrusters relative to the first one was demonstrated using simulations. It was clearly demonstrated that the second impulse from a pair of impulsers can be used to completely stop the projectile's angular motion, thus limiting range lost, while contributing to the drift correction at the same time. Finally, it was shown that significant drift correction could be obtained for an artillery projectile if the three rules were applied in determining the location, roll orientation and timing of the impulses.

References

[1]Champigny, P. and Lacau, R.G. 1994. "Lateral Jet Control for Tactical Missiles," AGARD-R-804, Missiles Aerodynamics.

[2]Brandeis, J. and Gill, J. 1998. "Experimental Investigation of Super- and Hypersonic Jet Interaction on Missile Configurations," Journal of Spacecraft and Rockets, Vol. 35, No. 3, pp. 296-302.

[3]Wey, P., Berner, C., Sommer, E., Fleck, V. and Moulard, H. 2005. "Theoretical Design for a Guided Supersonic Projectile," presented at the 22nd International Symposium on Ballistics, Vancouver, BC.

[4]Horwath, T.G. and Barnych, G. 2004. "Low Cost Course Correction (LCCC) Technology Applications," presented at the NDIA International Armaments Technology Symposium, Parsippany, NJ.

[5]Magnotti, P.J., Terhune, J. and Barnych, G. 2003. "Low Cost Course Correction (LC3) For Mortars Information Briefing," presented at the 38th Annual Gun, Ammunition and Missiles Symposium & Exhibition, Monterey, CA.

[6]Cooper, G.R. 2003. "Projectile Aerodynamic Jump Due to Lateral Impulsives," ARL-TR-3087.

[7]Burchett, B., Peterson, A. and Costello, M. 2002. "Prediction of Swerving Motion of a Dual-Spin Projectile With Lateral Pulse Jets in Atmospheric Flight," Mathematical and Computer Modelling, Vol. 35, No. 7, pp. 821-834.

[8]English, B.A., Gadiraju, P., Rinehart, C.S., Glezer, A. and Allen, M.G. 2006. "Gas Generator Actuator Arrays for Flight Control of Spinning Body Projectiles," Tech. Dig. 19th IEEE Int. Conf. MicroElectro Mechanical Systems (MEMS 2006), Istanbul, Turkey.

[9]Wey, P. and Corriveau, D. 2008. "Trajectory Deflection of Fin- and Spin-stabilized Projectiles Using Paired Lateral Impulses," presented at the 24th International Symposium on Ballistics, New Orleans, LA.

[10]McCoy, R.L. "Linearized Pitching and Yawing Motion of Rotationally Symmetric Projectiles", in *Modern Exterior Ballistics: The Launch and Flight Dynamics of Symmetric Projectiles.*

[11]McCoy, R.L. "Linearized Swerving Motion of Rotationally Symmetric Projectiles", in *Modern Exterior Ballistics: The Launch and Flight Dynamics of Symmetric Projectiles.*